THE
PHYSICAL REVIEW

A journal of experimental and theoretical physics established by E. L. Nichols in 1893

SECOND SERIES, VOL. 128, NO. 1 OCTOBER 1, 1962

Noise Radiation and Scattering from a Cylindrical Plasma Column

B. AGDUR, B. KERŽAR, AND F. SELLBERG
Microwave Department, Royal Institute of Technology, Stockholm, Sweden
(Received April 23, 1962)

Noise radiation and scattering from a cylindrical mercury discharge plasma at microwave frequencies are studied experimentally and theoretically as functions of the electron density. Measurements are made both in free space and in a waveguide system at different values of the gas density and for different polarizations of the electromagnetic field.

INTRODUCTION

BOTH noise radiation and scattering from plasma columns have been studied earlier.[1–3] However, the earlier measurements do not allow a direct comparison between the two. Most noise measurements are made at so high collision frequencies that the resonant properties of the plasma column have very little influence on the noise radiated, and the scattering measurements are generally made at rather low collision frequencies.

The measurements reported here allow a direct comparison between scattering and noise from a plasma column at different collision frequencies and for different polarizations of the microwave field. The electron density is measured by means of the microwave cavity technique. The theoretical calculations of back-scattering and absorption cross sections are based on the assumptions that inhomogeneities in the plasma density can be neglected and that the temperature of the electrons is only introduced indirectly through the collision frequency. The influence of the glass walls surrounding the plasma column is taken into account.

Measurements of scattering and noise from a plasma should, ideally, provide an easy method to determine some important properties of the plasma. Very large discrepancies between theory and experiments are, however, observed and one of the purposes of the investigation reported here is to get a more complete picture of the phenomenon.

[1] D. Romell, Nature **167**, 243 (1951).
[2] A. Dattner, Ericsson Techniques **13**, 309 (1957).
[3] B. Agdur and B. Enander, J. Appl. Phys. **33**, 575 (1962).

EXPERIMENTAL SETUP

The plasma studied was the positive column of a mercury discharge. It had a length of 150 cm and a 12.8-mm diam in the free space experiments and a length of 30 cm and a 12.8-mm diam in the waveguide experiments. The wall thickness of the glass tube was 1.4 mm. The mercury gas pressure was controlled by the temperature of the mercury pool, and the glass tube surrounding the plasma column was kept at a constant temperature well above that of the mercury pool. The temperature of the mercury pool could be varied between 10 and 60°C, corresponding to a pressure variation from 0.5×10^{-3} to 25×10^{-3} mm Hg. The electron density was measured by means of the microwave cavity method; the cavity operated in the TM_{010} mode and the resonant frequency of the empty cavity for this mode was 1760 Mc/sec.

A sensitive receiver of the radio astronomy type was used for the noise measurements, Fig. 1. In the waveguide measurements the receiver was connected to a terminated waveguide in which the plasma tube was placed as shown in Fig. 2. In the free space measurements the noise radiated from the plasma column was picked up by a horn antenna. The receiver was operating at a frequency of 3300 Mc/sec and had a bandwidth of 20 Mc/sec. The lowest detectible power was 10^{-17} W. The calibration of the receiver was done with a standard noise source and a calibrated precision attenuator.

The scattering was studied at the same frequency as the noise. The antenna arrangement for the free space case is shown in Fig. 3. In the waveguide scattering experiments the power was fed to the plasma tube

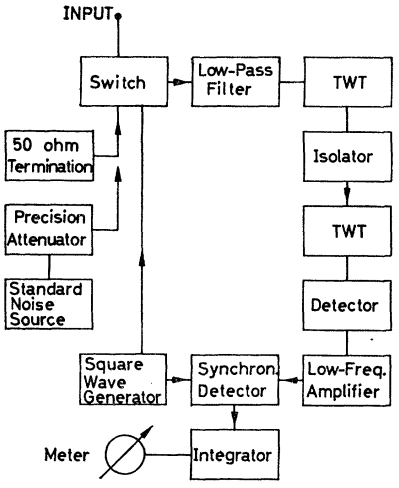

FIG. 1. Block diagram of the sensitive microwave receiver.

through a directional coupler as shown in Fig. 2. In the free space measurements the polarization of the fields could be changed and the receiving antenna could be rotated with the plasma column as axis in order to measure the azimuthal distribution of the scattered energy.

THEORY

The theoretical calculations of backscattering and absorption cross sections are made on the assumption of a homogeneous plasma. Collision damping is introduced by assuming that the plasma can be described as a dielectric with the complex dielectric constant

$$\left[1-\frac{(\omega_p/\omega)^2}{(1-j\nu/\omega)}\right],$$

where ω_p is the plasma frequency and ν is the electron collision frequency. The temperature of the electrons enters only indirectly through the collision frequency.

The influence on the field distribution of the glass wall surrounding the plasma column is taken into account. The fields are assumed to have a constant phase along the plasma column, i.e., scattering and absorption are calculated for a plane wave which propagates perpendicular to the plasma column.

The ratio between emissivity and absorptivity is a constant for a body in thermal equilibrium. The plasma is assumed to be in thermal equilibrium so that the radiated noise power is proportional to the absorption diameter.

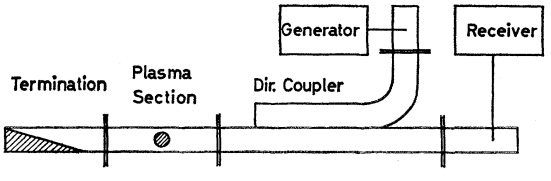

FIG. 2. Waveguide system for scattering and noise measurements.

The formulas on which the theoretical curves are based are given in the Appendix.

EXPERIMENTAL AND THEORETICAL RESULTS

Scattering in the Free Space System

The results obtained for the free space system are given in Figs. 4 and 5. The solid curves in Figs. 4(a), 4(b), and 4(c) show the energy scattered from the plasma column as a function of plasma density. The three different sets of curves show the behavior of the system at three different gas densities: $N_{g1}=2.6\times10^{19}$, $N_{g2}=2.6\times10^{20}$, and $N_{g3}=6.2\times10^{20}$ m^{-3}. The mean free paths, λ_e, and the collision frequencies, η, corresponding to these gas densities are $\lambda_{e1}=95$, $\lambda_{e2}=7$, $\lambda_{e3}=2.2$ mm and $\nu_1=14$, $\nu_2=130$, $\nu_3=400$ Mc/sec.

The electric vector of the incident wave was perpendicular to the plasma column and the receiving antenna was oriented to receive only this polarization direction. The experiments show that, in contradiction to the theory, there are two large scattering maxima. When

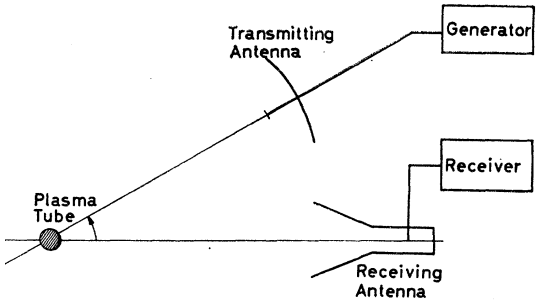

FIG. 3. Free space system for scattering and noise measurements.

the gas density is increased, the scattering maximum occurring at the lower plasma frequency increases in amplitude whereas the second maximum slowly decreases. The curves also show that the observed scattering maxima move to higher plasma frequencies as the gas density is increased. In contrast with this, the plasma frequency at which the theory predicts a large scattering is almost independent of the gas density.

The solid curves in Figs. 5(a), 5(b), and 5(c) show the theoretically determined backscattered power for the following collision frequencies: 20, 200, and 2000 Mc/sec. At collision frequencies above 200 Mc/sec the dipole mode is predominant in determining the scattered energy. The quadrupole mode appears at very low collision frequencies as a dip in the curve showing the scattered energy vs plasma frequency. The figure indicates that the scattering dip due to the quadrupole mode appears at higher plasma density than the scattering maximum for the dipole mode. This is due to the influence of the glass wall; if this was not taken into account the dip would occur at lower plasma density. It should be mentioned that at low neutral

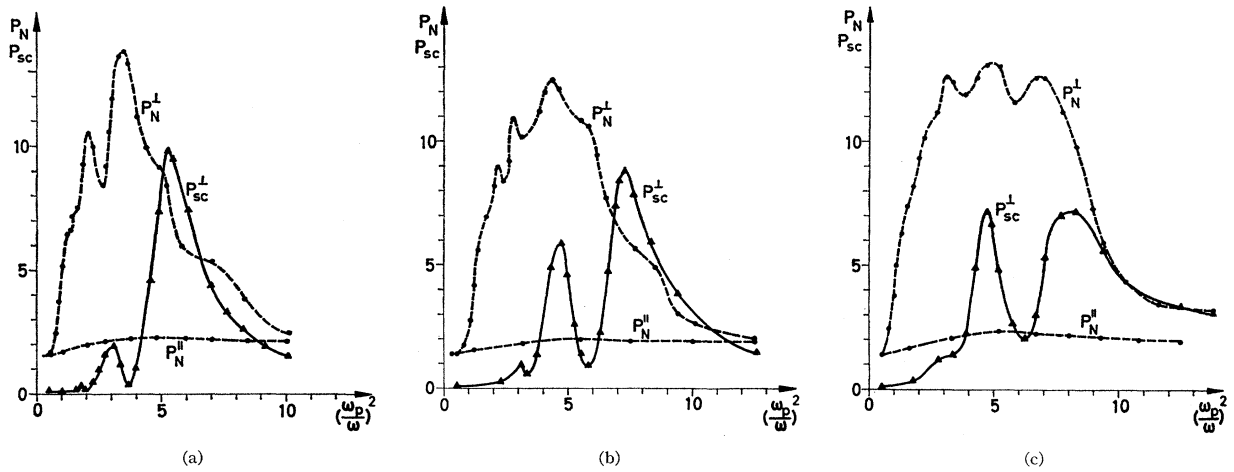

FIG. 4. Variation of scattered power, P_{sc}, and noise power ,P_N, with plasma frequency obtained in free space measurements. Power in arbitrary units. (a) $\lambda_e=95$ mm, $\nu=14$ Mc/sec. (b) $\lambda_e=7$ mm, $\nu=130$ Mc/sec. (c) $\lambda_e=2.2$ mm, $\nu=400$ Mc/sec.

gas densities the electrons collide more frequently with the glass walls than with the gas molecules and it is, therefore, very doubtful if the theoretical curve for the lowest collision frequency, corresponding to a mean free path of 6 cm, has any significance. It should also be pointed out that the theory is based on the assumption that the waves have the same phase along the plasma column. When the plasma is illuminated by a microwave beam of finite size it is obvious that the phase of the fields will not be constant along the column.

The electron density is determined with the microwave cavity method. The shift in the resonant frequency of the cavity caused by the presence of the electrons is measured and the plasma density is calculated. It is important to point out that, at low plasma densities, the frequency shift for the TM_{010} mode depends only on the mean value of the plasma density and not on the density distribution. At high plasma densities, however, both the mean value of the electron density and the distribution of the density influence the frequency shift. In our calculation of the plasma frequency we have assumed that the electron density has a rectangular distribution. For a parabolic distribution of electron density, the scattering maxima would occur at higher mean values of the plasma frequency than for the rectangular distribution. This difference in the mean value of the plasma frequency between the rectangular and parabolic distribution increases as the plasma density increases.[3]

The azimuthal distribution of the scattered energy was studied by means of the arrangement shown in Fig. 3. The measurements showed that the scattered field has a dipole character for both the main scattering maxima observed.

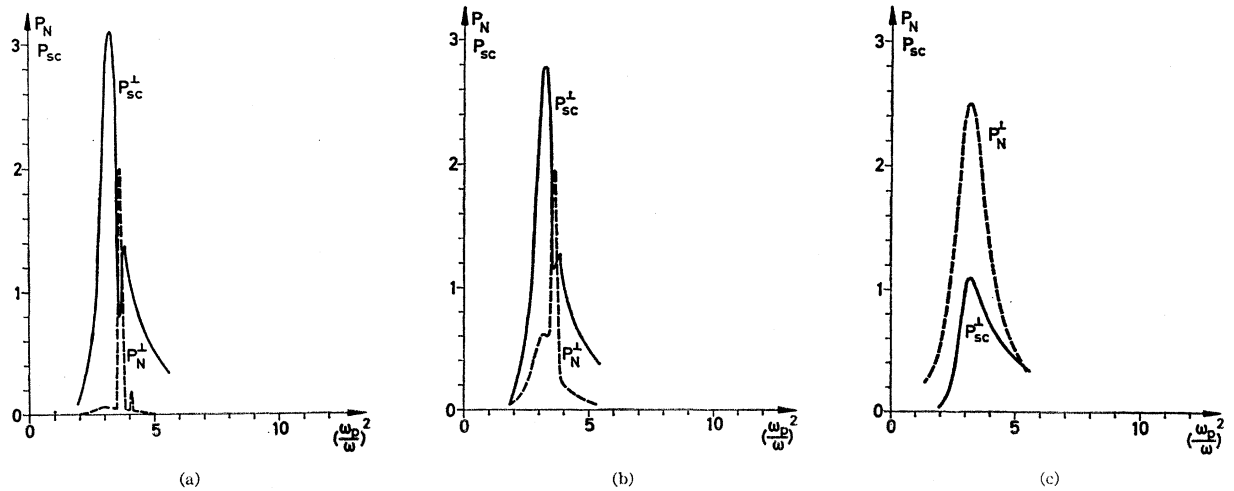

FIG. 5. Theoretically determined variation of scattered power, P_{sc}, and noise power, P_N, with plasma frequency. Power in arbitrary units. (a) $\nu=20$ Mc/sec. (b) $\nu=200$ Mc/sec. (c) $\nu=2000$ Mc/sec.

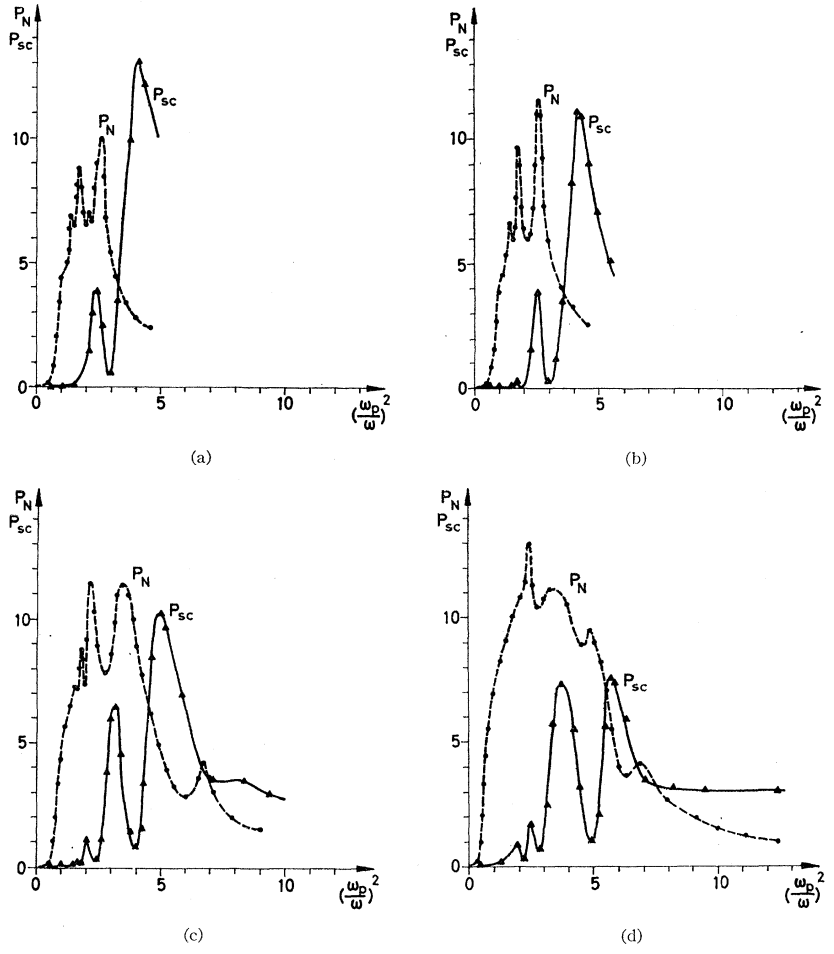

FIG. 6. Variation of scattered power, P_{sc}, and noise power P_N, with plasma frequency obtained in waveguide measurements. Power in arbitrary units. (a) $\lambda_e=70$ mm, $\nu=19$ Mc/sec. (b) $\lambda_e=25$ mm, $\nu=44$ Mc/sec. (c) $\lambda_e=7$ mm, $\nu=130$ Mc/sec. (d) $\lambda_e=1.8$ mm, $\nu=500$ Mc/sec.

Noise Power Radiated in the Free Space System

The dashed curves in Fig. 4 show the noise power radiated from the plasma for the two cases where the electric field vector is perpendicular and parallel, respectively, to the plasma column. It is seen that the noise is strongly polarized perpendicular to the plasma column within a certain range of plasma frequency. The theory predicts such a polarization but for a much smaller range of plasma frequency. The curves of noise power vs plasma frequency show a fine structure but no large variations of the type that was observed in the scattered energy.

The dashed curves in Fig. 5 show theoretically calculated curves of noise power vs plasma frequency for three different values of collision frequency 20, 200, and 2000 Mc/sec. At collision frequencies below 800 Mc/sec the quadrupole mode will predominate in the noise radiation. The range of plasma frequencies with high noise power is very narrow. At the lowest gas densities used in the experiments the electrons will collide more frequently with the walls than with gas molecules and the theoretically calculated absorption cross sections for these gas densities may have no significance. It could be mentioned that if the collisions with the walls are assumed to be elastic, the noise originating in these collisions would also be polarized with the electric vector perpendicular to the plasma tube.

The Waveguide System

The results of the measurements of noise radiation and scattering in the waveguide system are given in Fig. 6. The scattering and noise radiation were measured at four gas densities: $N_{g1}=3.5\times10^{19}$, $N_{g2}=9\times10^{19}$, $N_{g3}=2.6\times10^{20}$, and $N_{g4}=7.5\times10^{20}$ m^{-3} corresponding to the following collision frequencies: $\nu_1=19$, $\nu_2=44$, $\nu_3=130$, and $\nu_4=500$ Mc/sec. The general shapes of the curves, which show the noise power and the scattered power as functions of plasma frequency, are similar to the shapes of the corresponding curves obtained for the free space system. However, scattering and noise radiation occur at lower plasma densities in the waveguide than in the free space system, and there are also some differences in the "fine" structure of the curves.

APPENDIX

Scattering and absorption of a plane wave by a plasma column surrounded by a glass tube are studied theoretically under the assumptions previously described.

The incident plane wave is expanded in cylindrical waves by applying the identity

$$\exp\left(-j\frac{\omega}{c}y\right)=\exp\left(-j\frac{\omega}{c}r\sin\varphi\right)$$

$$=\sum_{n=-\infty}^{+\infty}J_n\left(\frac{\omega r}{c}\right)\exp(-jn\varphi).$$

The induced fields in the plasma, glass tube, and surrounding space are added, and the total field is finally made consistent by applying the continuity conditions at the different boundaries.

For perpendicular polarization of the incident electric field vector one gets the following formulas for scattered and absorbed power:

$$\frac{r}{r_0}P_{sc}\perp=\frac{2}{\pi(\beta_0r_0)}\left|\sum_{n=-\infty}^{+\infty}(-1)^n\times\frac{(b_nc_n-a_ne_n)}{(b_nc_n-a_ne_n)+j(a_nf_n-b_nd_n)}\right|^2,$$

$$\frac{Q_a\perp}{2r_0}=\frac{16}{\pi^3\epsilon_2(\beta_0r_0)^2(\beta_0r_1)^2}\times\mathrm{Im}\left[\sum_{n=-\infty}^{+\infty}\frac{(\epsilon_1^{1/2})^*J_n'(\epsilon_1^{1/2}\beta_0r_0)J_n^*(\epsilon_1^{1/2}\beta_0r_0)}{|(b_nc_n-a_ne_n)+j(a_nf_n-b_nd_n)|^2}\right],$$

where

$P_{sc}\perp$ = the backscattered power density for perpendicular polarization normalized to incident power density 1,

$Q_a\perp$ = the absorption diameter for perpendicular polarization,

r_0 = radius of the plasma cylinder,

r_1 = outer radius of the glass tube,

$\beta_0=\omega/c$ = phase constant of free space,

$\epsilon_1=[1-(\omega_p/\omega)^2/(1-j\nu/\omega)]$ = equivalent dielectric constant of the plasma,

ϵ_2 = dielectric constant of the glass tube,

ω_p = electron plasma frequency,

ν = electron collision frequency,

$$a_n=J_n(\epsilon_2^{\frac{1}{2}}\beta_0r_0)J_n'(\epsilon_1^{\frac{1}{2}}\beta_0r_0)-(\epsilon_1/\epsilon_2)^{\frac{1}{2}}J_n'(\epsilon_2^{\frac{1}{2}}\beta_0r_0)J_n(\epsilon_1^{\frac{1}{2}}\beta_0r_0),$$

$$b_n=Y_n(\epsilon_2^{\frac{1}{2}}\beta_0r_0)J_n'(\epsilon_1^{\frac{1}{2}}\beta_0r_0)-(\epsilon_1/\epsilon_2)^{\frac{1}{2}}Y_n'(\epsilon_2^{\frac{1}{2}}\beta_0r_0)J_n(\epsilon_1^{\frac{1}{2}}\beta_0r_0),$$

$$c_n=\epsilon_2^{\frac{1}{2}}J_n(\epsilon_2^{\frac{1}{2}}\beta_0r_1)J_n'(\beta_0r_1)-J_n'(\epsilon_2^{\frac{1}{2}}\beta_0r_1)J_n(\beta_0r_1),$$

$$d_n=\epsilon_2^{\frac{1}{2}}J_n(\epsilon_2^{\frac{1}{2}}\beta_0r_1)Y_n'(\beta_0r_1)-J_n'(\epsilon_2^{\frac{1}{2}}\beta_0r_1)Y_n(\beta_0r_1),$$

$$e_n=\epsilon_2^{\frac{1}{2}}Y_n(\epsilon_2^{\frac{1}{2}}\beta_0r_1)J_n'(\beta_0r_1)-Y_n'(\epsilon_2^{\frac{1}{2}}\beta_0r_1)J_n(\beta_0r_1),$$

$$f_n=\epsilon_2^{\frac{1}{2}}Y_n(\epsilon_2^{\frac{1}{2}}\beta_0r_1)Y_n'(\beta_0r_1)-Y_n'(\epsilon_2^{\frac{1}{2}}\beta_0r_1)Y_n(\beta_0r_1),$$

the prime indicates differentiation with respect to the argument, and the asterisk indicates complex conjugate value.

The parameter values used for the theoretical curves in Fig. 5 are

$$\beta_0r_0=0.4,\quad r_0/r_1=0.8,\quad \epsilon_2=4;$$
$$\nu/\omega=0.001,\quad 0.01,\quad \text{and}\quad 0.1,$$

corresponding to

$$\nu=20,\ 200,\ \text{and}\ 2000\ \text{Mc/sec},$$

respectively.

ACKNOWLEDGMENT

The authors are greatly indebted to K. Abrahamsen for his skillful technical assistance.